ISSN 2543-9901

JOURNAL OF CASTING & MATERIALS ENGINEERING

AGH UNIVERSITY OF SCIENCE AND TECHNOLOGY
FACULTY OF FOUNDRY ENGINEERING

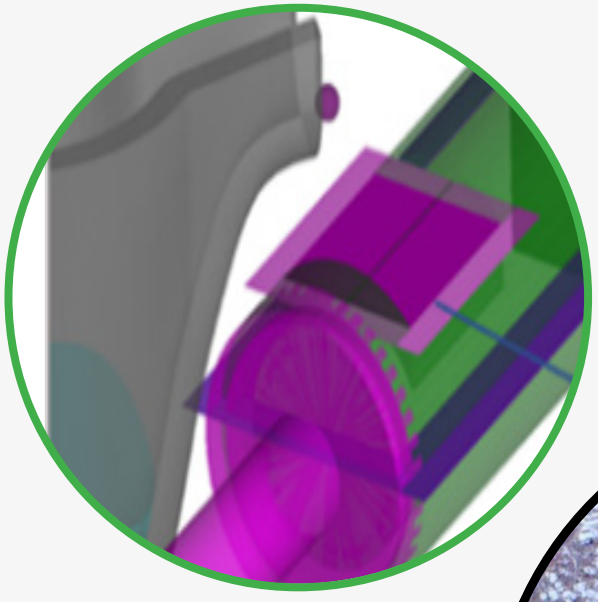

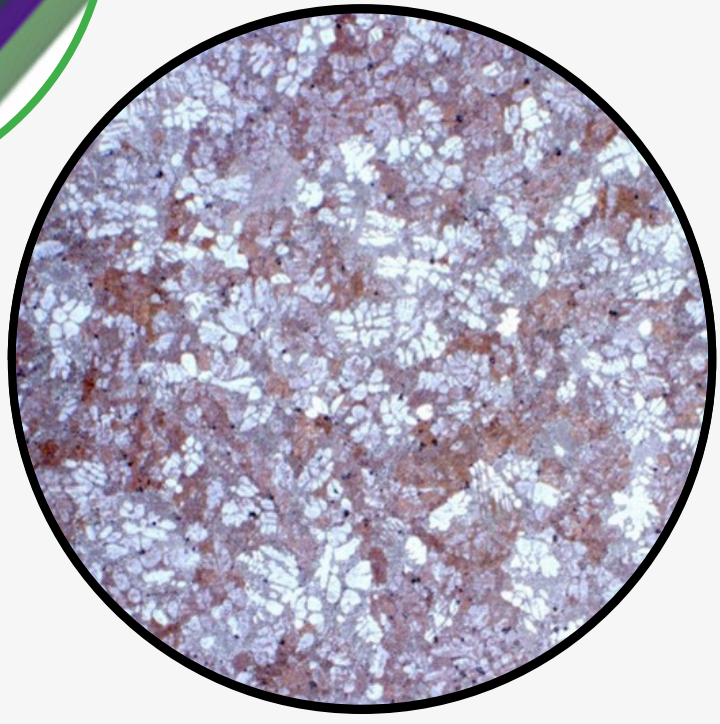

QUARTERLY
Vol. 6 No. 3/2022

JCME

AGH UNIVERSITY PRESS
KRAKOW 2022

The articles published in the Journal of Casting & Materials Engineering have been given a favorable opinion by the rewievers designated by the Editorial Board.

www:
https://journals.agh.edu.pl/jcme/

AGH UNIVERSITY PRESS KRAKOW 2022

Wydawnictwa AGH (AGH University Press)
al. A. Mickiewicza 30, 30-059 Kraków
tel. 12 617 32 28, 12 638 40 38
e-mail: redakcja@wydawnictwoagh.pl
http://www.wydawnictwa.agh.edu.pl

Contents

Journal of Casting & Materials Engineering Vol. 6 No. 3 (2022) 58–63
https://doi.org/10.7494/jcme.2022.6.3.58

The Influence of Cooling Rate on the Damping Characteristics of the ZnAl4Cu1 Alloy

Grzegorz Piwowarski*, Beata Gracz

AGH University of Science and Technology, Faculty of Foundry Engineering, 23 Reymonta St., 30-059 Krakow, Poland
e-mail: piwgrz@agh.edu.pl

Received: 3 February 2022/Accepted: 27 July 2022/Published online: 8 August 2022.
This article is published with open access at AGH University of Science and Technology Journals.

Abstract

The paper presents the results of damping coefficient tests on the ZnAl4Cu1 alloy (ZL5). The damping coefficient has been calculated on the basis of specimen measurements obtained with the use of the signal echo method. The method consists in passing an ultrasonic wave through the tested material. The ultrasonic wave from a transmitting and receiving head passes through a specimen, bounces off its bottom surface and comes back to the measuring head in the form of a signal echo. The difference in the signal intensity between the first and the second echo in relation to the distance travelled by the ultrasound wave is a value of the material's damping characteristics. The specimens were cast into three molds made of different materials, i.e. green sand, plaster and metal. The thermophysical properties of these materials are different, affecting the rate of heat absorption from the cast. Three series of specimens have been obtained which have different cooling rates. The specimens were then subjected to ultrasound and microscopic tests to assess the alloy structure. The internal alloy structure affects its damping properties to a great extent.

Keywords:

zinc alloys, damping coefficient, damping capacity, high-damping metals, cooling rate, ultrasound testing

1. INTRODUCTION

Zinc-aluminum alloys, as well as ternary zinc-aluminum-copper alloys, can be used in less loaded machine parts and structural components. Due to their relatively low melting temperature, the energy consumption necessary to produce components from those alloys is reduced while they still maintain good corrosion resistance and high damping properties. Zinc alloys have the ability to dampen vibration, placing them in the group of HIDAMETS (High-Damping Metals), together with cast iron and bronzes [1, 2]. A parameter indicating the damping properties of a specific material is the damping coefficient α. The coefficient's value depends on the type and composition of the alloy. In general, the damping properties of a specific alloy are mostly determined by its internal structure [3, 4]. The value of the damping coefficient of an alloy with a specified chemical composition is constant. It can be changed, however, in the process of alloy modification, a process which usually affects the volume and number of precipitation of a specific compound or the size of grain. The inoculant's impact on the alloy structure is reflected in the change of the damping coefficient value of a specific alloy [5–7]. The cooling rate, apart from modification process, can also affect the macro and microstructure of the alloy by the changing shape and grain size of the phases [8–10]. The microstructure of an alloy influences its properties. The grain size and structure of the alloy components affect the ability of the alloy to dampen vibrations. A coarse-grained structure with large, branched dendrites also exhibits a better corrosion resistance tendency than finer grain structures. It is most often caused by corrosion centers at the grain boundaries. The more boundaries, the more places where a significant difference in corrosion potential can occur [11–13]. Zinc-aluminum based alloys, due to their lower component and production costs, often replace bronze in wear-resistant components. They work well for less loaded components operating at lower temperatures. The tribological properties of zinc alloys decrease at temperatures above 100°C. The addition of copper increases the hardness, strength and wear resistance of Zn-Al alloys up to a content of 2-wt.%. Changes in the size of ingredients in the alloy structure also affect the wear resistance. Zinc-aluminum alloys with a finer structure display higher wear resistance and hardness [4, 14, 15].

This paper describes an attempt to measure the damping coefficient of the ZnAl4Cu1 (ZL5) alloy solidified at three different cooling rates. In order to obtain three different cooling rates, the tested alloy was cast into molds made of various materials characterized by different thermophysical properties. The

damping coefficient indicates the material's ability to absorb and scatter vibration. In perfect materials, the vibrating wave passes the material without any loss of its energy. In particular castings which are relatively heterogeneous in terms of their internal structure, the vibrating wave becomes attenuated. It is partially absorbed by the material and converted into other types of energy, mainly thermal, but primarily the energy of vibrations is dispersed on compounds of the alloy structure. The paper describes a test in which an ultrasonic wave has been used to determine the damping properties of the ZL5 alloy. The principle of ultrasonic wave measurements is based on physical properties of the materials being tested and also on the properties of the ultrasound waves themselves. Ultrasonic waves are very well propagated in solids such as metals. Examining an ultrasonic wave which has passed through the material or has been reflected from the specimen provides information regarding to any irregularities in material continuity. At the beginning of the usage of ultrasounds in foundry engineering, ultrasonic waves were only used to locate defects in castings. With the progress of technology, they were found to be useful in measurements of material thickness, determining microstructure and examining the ability of a specific material to dampen vibrations. Due to the use of an ultrasonic wave, tests of damping properties can be performed in a simple and fast manner. Transmitter--receiver heads are characterized by small diameters, facilitating the testing of small specimens. In order to eliminate the signal loss, the surface of a tested specimen should be smooth and even. At the point of contact between the transmitter--receiver head and the specimen, a coupling liquid needs to be used to transmit the transverse and longitudinal ultrasonic waves to the test material. The correct selection of the wavelength is another important factor. If the emitted wavelength from the measuring instrument is not matched to the diameter of the average grain, structural noise may occur, especially in the case of large grains. Structural noise is often the source of interference in damping measurements. To prevent those phenomena, it is recommended to use ultrasonic waves at least six times longer than the average grain size of the tested material [16, 17].

The aim of the research is to determine the influence of the cooling rate of the ZL5 alloy on its microstructure and vibration damping properties. Typically, the literature finds the damping properties of zinc alloys cast into a metal mold and occasionally cast into one type of mold and inoculated. There are no comparisons of the test results for the damping properties of a specific alloy depending on the mold material. The mold material determines the cooling rate of the alloy, and thus affecting its properties. The damping properties depend on the alloy microstructure. The microstructure can be shaped by modifying or changing the cooling rate. In the case under consideration, it is proposed to determine the damping properties of the alloy for three different cooling rates. Alloys of this type are often cast into permanent molds, but also into sand molds. The use of a plaster mold in this case is intended to extend the results by a slow cooling. The type of mold material determines the cooling rate of the casting. The article shows the relationship between the cooling rate and the damping properties of the alloy which may be technologically useful.

2. EXPERIMENTAL PROCEDURE

The ZL5 alloy of composition shown in Table 1 was melted in a resistance crucible furnace in a graphite crucible. The furnace was heated to the temperature of 500°C. The batch was 3 kg of ZL5 alloy. After melting, the alloy was poured into three different types of molds (Fig. 1):

- a classical dry green sand mold,
- a plaster mold made of casting jewelry gypsum,
- a metal mold made of common steel preheated to a temperature of 100°C.

The molds had a cylindrical cavity with a diameter of 40 mm and a height of 100 mm. Two specimens were obtained from each type of the mold. During pouring and solidification of the cast, temperature measurements were taken. Data collected in such a manner was subsequently used to determine cooling curves and cooling rates. The temperature was taken with the use of a type K thermocouple placed in the cast axis. The thermocouple was located at the mid-height of the cast.

After cooling, specimens with a diameter of 40 mm and a height of 30 mm were cut out from the selection beneath the thermocouple of the castings.

Table 1
Chemical composition of the ZL5 alloy

Element	Al	Cu	Mg	Pb	Cd	Sn	Fe	Ni	Si	Zn
Composition [%]	4.06	0.91	0.05	0.003	0.001	0.001	0.022	0.001	0.002	The rest

Fig. 1. Types of foundry mold used in the experiment: dry green sand mold, plaster mold, metal mold

The specimens were ground with a 1000 grit abrasive paper and then tested to determine the damping coefficient. Ultrasound tests were performed with the transmitter-receiver head from the Krautkramer 2000 ultrasound testing kit. To improve contact between the transmitter-receiver head and the specimen surface, a paraffin oil was used (Fig. 2).

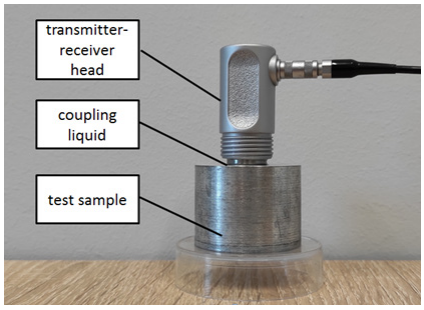

Fig. 2. Transmitter-receiver head on the tested sample

A longitudinal ultrasonic wave with a frequency of 1 MHz was applied and the specimens were tested using the echo method. A signal emitted from the transmitter-receiver head passed through the specimen bounced off its bottom and came back to the measuring head. As a result of signal dispersion and absorption by the compounds of alloy structure, it returned in the form of a weakened echo (Fig. 3).

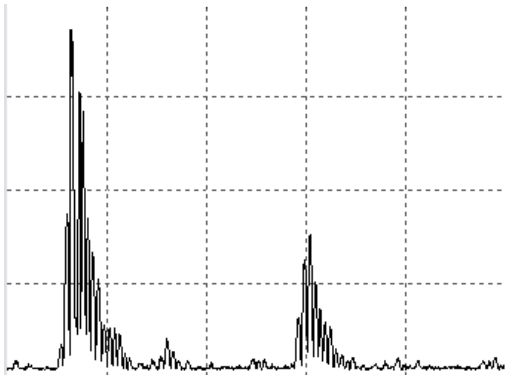

Fig. 3. One of the examples of the first and the second echo of the ultrasonic signal for tested ZL5 alloy

For each two specimens of a series, 10 measurements were performed which was necessary due to the heterogeneous structure of such material as a casting. The specimens were examined at a temperature of 22°C. After the collection of all the data, the average damping coefficient α was calculated for each specimen (Eq.(1)).

$$\alpha = \frac{P_1 - P_2}{2H}\left[\frac{\text{dB}}{\text{m}}\right] \tag{1}$$

where:

P_1, P_2 – the value of the first and second echo of the signal,
H – the height of the sample.

After the ultrasound tests, specimens were polished and etched in the Palmerton's reagent [18] for 20 s. The etching revealed the alloy structure which was observed via bright-field microscopy.

3. RESULTS OF THE INVESTIGATION

The data collected during solidification in the molds made of different materials has been presented in the form of cooling curves to be seen in Figure 4. The cooling rate of the casting for each specimen has also been determined. The data was selected in the range from the moment of pouring the mold to the moment of the start of the solidification process. In the metal mold heated to the temperature of 100°C, the alloy cooled down at the rate of approx. 9.3 K/s. In the case of the green sand mold with a quartz sand matrix, dried up before casting, the cooling rate was approx. 1 K/s. The lowest cooling rate was observed in the casting gypsum mold and it was approx. 0.37 K/s. The cooling rate is clearly visible from the slope of the cooling curves. The greater the slope and the shorter the time to reach a given temperature, the faster the cooling rate. This is clearly seen in Figure 4, when the curve for samples cooling the fastest (metal form) and the curve for samples cooling the slowest (plaster mold) are compared. In order to illustrate the shape of the curve cooling at high speed in a metal form, an additional graph is provided in Figure 4.

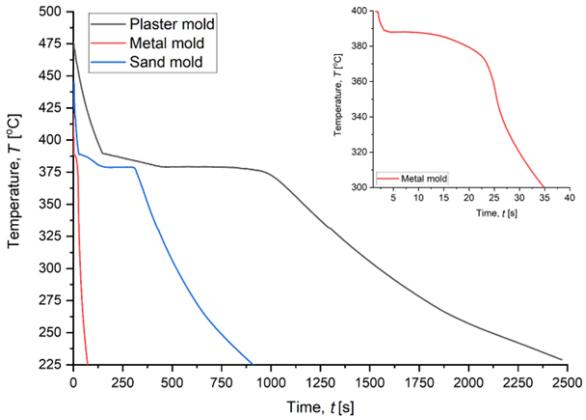

Fig. 4. Cooling curves of ZnAl4Cu1 alloy

The calculated damping coefficient α values are shown in Figure 5 and in Table 2.

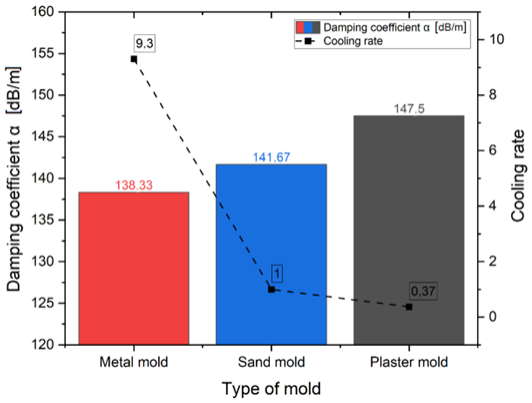

Fig. 5. Values of damping coefficient α related to the cooling rate

Table 2
The calculated damping coefficient α in relation to cooling rate, type of mold material and HB

Type of mold	Cooling rate [K/s]	Damping coefficient α [dB/m]	HRB
Plaster mold	0.37	147.50	97
Sand mold	1.00	141.67	94
Metal mold	9.30	138.33	104

The measured results indicate that the best damping properties have been achieved for the specimens in the gypsum mold, which solidified under the slowest heat removal condition. The lowest value of damping coefficient α was achieved for measurements performed on specimens cast in the metal mold, i.e. where the cooling rate was the highest. The difference between the best and worst result of damping properties is 9.17 dB/m. A hardness test was also performed for the tested samples. Hardness was measured by means of the Brinnell method. The diameter of the indenter was 2.5 mm. The applied force is 147 N. The hardness measurements results are presented in Table 2. As can be seen, there is no direct correlation between the cooling rate, the damping factor, and the hardness. Only for the highest cooling rate we observe the lowest value of the damping coefficient and the highest hardness. It is undoubtedly related to the presence of the finest alloy microstructure (Fig. 6).

Microscopic examination resulted in obtaining micrographs for the alloy based on different cooling rates. Microstructures are shown in Figures 6–8 in magnification 50× and 200×. The figures show the bright dendrites of the η phase (solid solution) against the background of the eutectic phase (α + η) visible by the lamellar grain pattern. The components of the microstructure of the ZnAl4Cu1 alloy poured into a dried green sand mold in magnification 200× show on Figure 9. As can be seen in the photos, the cooling rate affects all the components of the microstructure under different magnification. For the highest cooling rate of 9.3 K/s obtained in a metal form, we observe the smallest dendrites of the *n* solution and also the greatest fragmentation of the eutectic. Along with the reduction of the cooling rate to 0.37 K/s obtained in the gypsum form, we observe the largest dimension of the solution and eutectic dendrites. For the cooling rate of 1 K/s obtained in the dried sand form, the microstructure components are of average size. The cooling rate is determined by the type of mold material, which can also be clearly seen in the graph of the cooling curves (Fig. 4). The cooling rate directly affects the shape and size of the separate phases. This translates directly into the ability of the alloy to damp vibrations, which is presented in the comparison of the cooling rate and the values of the vibration damping coefficient in Table 2.

a) b)

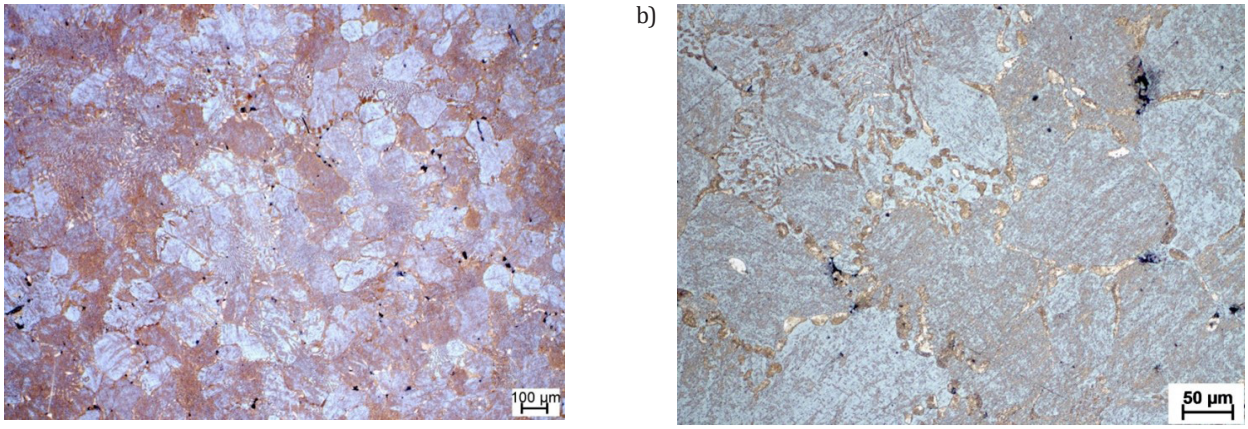

Fig. 6. Microstructure of ZnAl4Cu1 alloy cooling in the casting gypsum mold, magnification: a) 50×; b) 200×

a) b)

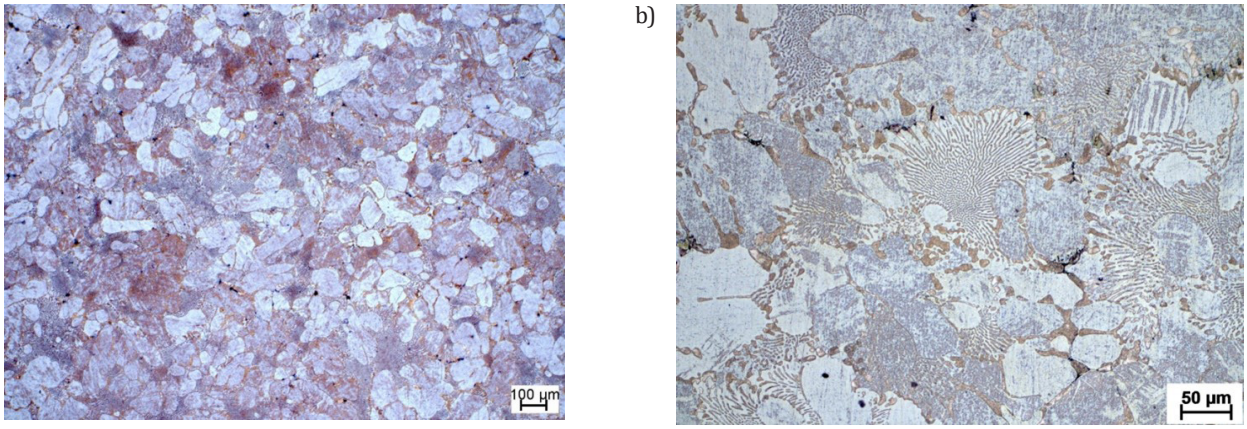

Fig. 7. Microstructure of ZnAl4Cu1 alloy cooling in the dried green sand mold, magnification: a) 50×; b) 200×

a) b)

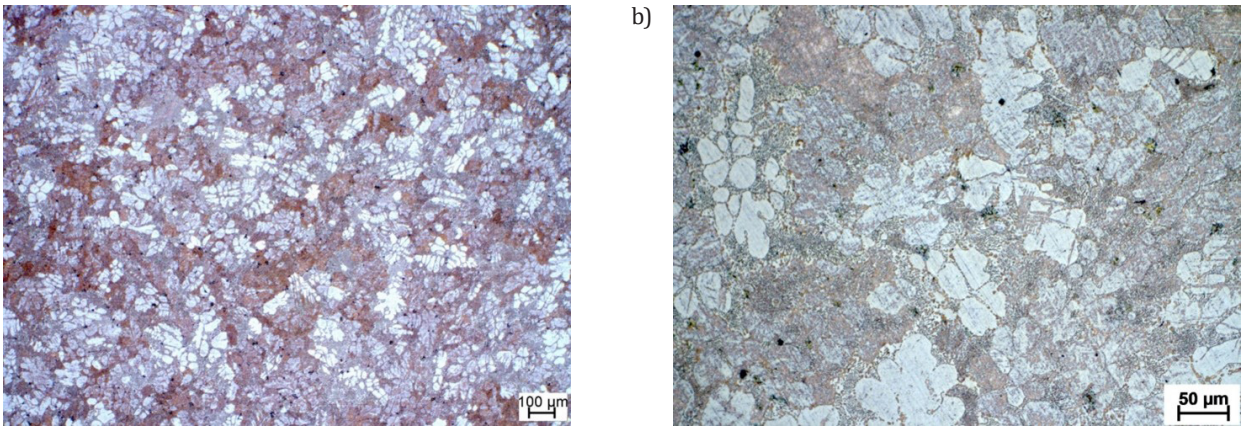

Fig. 8. Microstructure of ZnAl4Cu1 alloy cooling in the metal mold heated to the temperature of 100°C, magnification: a) 50×; b) 200×

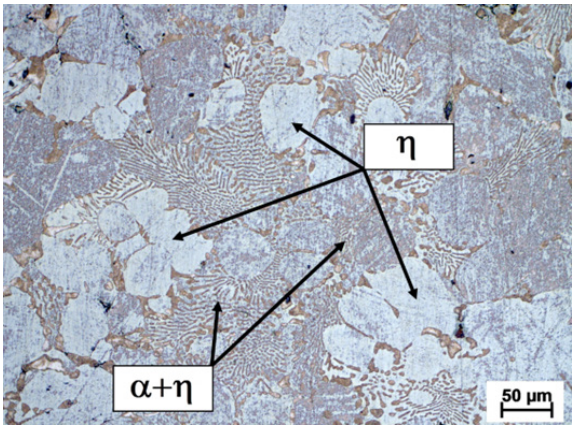

Fig. 9. Components of the microstructure of the ZnAl4Cu1 alloy poured into a dried green sand mold, magnification 200×

4. CONCLUSIONS

The ZnAl4Cu1 alloy cast into molds made of green sand, casting gypsum and steel solidified at different cooling rates. It can be perfectly seen on the distribution of cooling curves and is also evident from the calculated cooling rates. A low cooling rate obtained in the gypsum mold amounting to 0.37 K/s reflected for the values of the damping coefficient, which reaches to the highest value of 147.50 dB/m. In the gypsum mold we also have the most extensive phase η dendrites here, and the hardness here reaches an average value of 97 HB. The highest cooling rate was obtained for specimens solidifying in the metal mold, that is 9.3 K/s and the high cooling rate influences the microstructure. As we can see in the pictures (Figs. 6–8), the finest microstructure is in the sample of the metal mold (Fig. 6). For the specimens solidifying in the metal mold, the damping coefficient is α = 138.33 dB/m, the lowest value of all the samples. This means that the ZL5 alloy, which cools at a high cooling rate, has the lowest damping properties. However, the highest hardness is obtained here, amounting to 104 HB. This is the lowest value of a damping coefficient in this series of experiments. The specimens cast into the mold made of green sand, solidified at the cooling rate of 1 K/s. The value of the damping coefficient is 141.67 dB/m, and is between the aforementioned results for the plaster and steel molds. By controlling the cooling rate, we are able to influence the structure of the alloy, which affects its ability to subsequently dampen mechanical vibration. The results of the obtained damping coefficient α indicate that the ability to dampen vibrations increases for the tested ZL5 zinc alloy as the cooling rate decreases.

Acknowledgments

This work is financially supported by AGH University grant number: 16.16.170.654/B02.

REFERENCES

[1] Ritchie I.G. & Pan Z.-L. (1991). High damping metals and alloys. *Metallurgical Transactions A*, 22, 607–616. Doi: https://doi.org/10.1007/BF02670281.
[2] Ritchie I.G., Pan Z.-L. & Goodwin F.E. (1991). Characterization of the damping properties of die-cast zinc-aluminum alloys. *Metallurgical Transactions A*, 22, 617–622. Doi: https://doi.org/10.1007/BF02670282.
[3] Rzadkosz S. (1995). *Wpływ składu chemicznego i przemian fazowych na właściwości tłumiące i mechaniczne stopów z układu aluminium – cynk*. Rozprawy, Monografie. Kraków: Wydawnictwa AGH.
[4] Krajewski W.K. (2013). *Stopy cynku z aluminium. Rodzaje, właściwości, zastosowanie*. Kraków: Wydawnictwo Naukowe AKAPIT.
[5] Piwowarski G., Burać J. & Szucki M. (2017). Influence of AlTi3C0.15 modification treatment on damping properties of ZnAl10 alloy. *China Foundry*, 14(4), 292–296. Doi: https://doi.org/10.1007/s41230-017-7070-6.

[6] Krajewski W.K., Buraś J., Krajewski P.K. & Piwowarski G. (2015). Ultrasound wave attenuation of grain refined high-zinc aluminium sand-cast alloys. *Archives of Foundry Engineering*, 15(2), 51–54. Doi: https://doi.org/10.1515/afe-2015-0037.
[7] Krajewski W.K., Haberl-Faerber K., Buras J. & Krajewski P.K. (2012). Damping properties vs. Structure fineness of the high-zinc aluminum alloys. *Archives of Foundry Engineering*, 12(3), 63–66. Doi: https://doi.org/10.2478/v10266-012-0083-0.
[8] Lelito J., Żak P.L., Gracz B., Szucki M., Kalisz D., Malinowski P., Suchy J.S. & Krajewski W.K. (2015). Determination of substrate log-normal distribution in the AZ91/SiCp composite. *Metalurgija*, 54(1), 204–206.
[9] Górny M. & Sikora G. (2015). Effect of titanium addition and cooling rate on primary α(Al) grains and tensile properties of Al-Cu Alloy. *Journal of Materials Engineering and Performance*, 24(3), 1150–1156. Doi: https://doi.org/10.1007/s11665-014-1380-2.
[10] Shabestari S.G. & Malekan M. (2005). Thermal analysis study of the effect of the cooling rate on the mictrostructure and solidification parameters of 319 aluminum alloy. *Canadian Metallurgical Quarterly*, 44(3), 305–312. Doi: https://doi.org/10.1179/000844305794409409.
[11] Osório W.R., Freire C.M. & Garcia A. (2005). The effect of the dendritic microstructure on the corrosion resistance of Zn-Al alloys. *Journal of Alloys and Compounds*, 397, 179–191. Doi: https://doi.org/10.1016/j.jallcom.2005.01.035.
[12] Osório W.R., Freire C.M.A. & Garcia A. (2005). Dendritic solidification microstructure affecting mechanical and corrosion properties of a Zn4Al alloy. *Journal of Materials Science*, 40, 4493–4499. Doi: https://doi.org/10.1007/s10853-005-0852-z.
[13] Osório W.R., Spinelli J.E., Cheung N. & Garcia A. (2006). Secondary dendrite arm spacing and solute redistribution effects on the corrosion resistance of Al-10 wt% Sn and Al-20 wt% Zn alloys. *Materials Science and Engineering A*, 420, 179–186. Doi: https://doi.org/10.1016/j.msea.2006.01.058.
[14] Lachowicz M.M., Leśniewski T., Lachowicz M.B. & Jasionowski R. (2020). Tribological wear of as cast Zn-4Al alloy cooled at various rates from the eutectoid transformation temperature. *Archives of Foundry Engineering*, 20(4), 108–114. Doi: https://doi.org/10.24425/afe.2020.133356.
[15] Savaşkan T., Pürçek G. & Hekimoğlu A.P. (2003). Effect of copper content on the mechanical and tribological properties of ZnAl27-based alloys. *Tribology Letters*, 15(3), 257–263. Doi: https://doi.org/10.1023/A:1024817304351.
[16] Deputat J. (1979). *Badania ultradźwiękowe. Podstawy*. Gliwice: Instytut Metalurgii Żelaza.
[17] Deputat J., Mackiewicz S. & Szelążek J. (2007). *Problemy i techniki nieniszczących badań materiałów: wybrane wykłady*. Warszawa: Biuro Gamma.
[18] Petzow G. (1999). *Metallographic Etching. Techniques for Metallography, Ceramography, Plastographyk.* 2nd Ed. ASM International.

Journal of Casting & Materials Engineering Vol. 6 No. 3 (2022) 64–68
https://doi.org/10.7494/jcme.2022.6.3.64

The Effect of High Silicon and Molybdenum Content on the Mechanical Properties and Microstructure of Gray Cast Iron

Łukasz Dyrlaga[a, b,*], Dariusz Kopyciński[a], Edward Guzik[a], Grzegorz Soból[a], Dariusz Borak[b]

[a]AGH Univestity of Science and Technology, Faculty of Foundry Engineering, Reymonta 23 St., 30 059 Krakow, Poland
[b]METALPOL Węgierska Górka sp. z o.o., ul. Kolejowa 6, 34-350 Węgierska Górka, Poland
**e-mail: dyrlaga@agh.edu.pl*

Received: 7 February 2022/Accepted: 30 September 2022/Published online: 1 October 2022.
This article is published with open access at AGH University of Science and Technology Journals.

Abstract

This paper presents an overview of the current knowledge concerning SiMo ductile cast iron begins by describing the standard type of ductile cast iron before proceding to description of its microstructures. The paper then presents its chemical composition and the significant influence of individual elements on technological and mechanical properties. The research section focuses the influence of the addition of Si and Mo to the matrix of gray iron. After casting, stepped samples were carried out on the microstructure along with UTS tensile strength tests. The research presented in the article is a preliminary step towards the goal of obtaining a stable production process for silico-molybdenum cast iron.

Keywords:

SiMo cast iron, structure, mechanical properties, chemical composition, gray iron

1. INTRODUCTION

Increasingly, iron castings are required to withstand high temperatures, a phenomenon particularly visible in the production and operation of internal combustion vehicles. In this case, two types of loads can be distinguished that act on the cast parts of exhaust systems. The first is thermal loads and the second is thermochemical [1]. In addition, thermal loads can have a static effect on cast iron (heating up to a certain treatment temperature and withstanding it) and transiently (alternately heating and cooling machine parts) [2]. Modern internal combustion cars, in order to achieve the highest possible performance while reducing pollutants introduced into the atmosphere, are most often designed with turbines and exhaust gas collectors, and thus the temperature during operation can even reach over 1000°C [3]. Moreover, the casting itself may heat up unevenly during operation, which in turn leads to internal stresses [4]. In the production of machine parts exposed to these thermal loads SiMo ductile cast iron can be used, which retains the positive technological properties of classic nodular cast iron, while at the same time enjoying high thermal resistance [5]. The review of the current knowledge will allow the development of a technology for the production of SiMo cast iron castings in production conditions, as well as to adjust the process parameters in order to obtain a finished product of the highest quality. Factors such as chemical composition, the iron melting process, nodularization and inoculation should all be taken into account. In this paper we focus on the influence of increased content of silicon and molybdenum on the functional properties of gray cast iron to prevent the growth of unfavorable primary graphites [6]. As there is no mention of this type of cast iron in the literature, but only the corrosion resistance of high-silicon gray cast iron, the knowledge about SiMo ductile cast iron will serve as theoretical basis.

1.1. Grades and structure of SiMo ductile iron

SiMo cast iron grades were included in the EN 16124 standard. There are 9 grades of cast iron which, together with the silicon and molybdenum contents and the basic mechanical parameters, are presented in Table 1.

Molybdenum at higher contents causes perlite to appear in the matrix and this is not conducive to obtaining the appropriate mechanical properties. At 0.8% molybdenum, perlite with carbides appears between the ferrite grains [7].

Table 1
Symbols, chemical composition, and basic mechanical properties of SiMo ductile cast iron, based on [8]

Symbol	Chemical composition [%]		Tensile strength [MPa min.]	0.2% proof strength [MPa min.]	Elongation [% min.]	Brinell hardness
	Silicon	Molybdenum				HBW [1]
EN-GJS-SiMo25-5	2.3–2.7	0.4–0.6	420 [2]	260 [2]	12	140–210 [2]
			400 [3]	250 [3]		130–200 [3]
EN-GJS-SiMo30-7	2.8–3.2	0.6–0.8	440 [2]	310 [2]	10	150–220 [2]
			420 [3]	300 [3]		140–210 [3]
EN-GJS-SiMo35-5	3.3–3.7	0.4–0.6	440 [2]	330 [2]	8	160–230 [2]
			440 [3]	320 [3]		150–220 [3]
EN-GJS-SiMo40-6	3.8–4.2	0.5–0.7	480	380	8	190–240
EN-GJS-SiMo40-10		0.8–1.1	510	400	6	190–240
EN-GJS-SiMo45-6	4.3–4.7	0.5–0.7	520	420	7	200–250
EN-GJS-SiMo45-10		0.8–1.1	550	460	5	200–250
EN-GJS-SiMo50-6	4.8–5.2	0.5–0.7	580	480	4	210–260
EN-GJS-SiMo50-10		0.8–1.1	600	500	3	210–260

1) Approximate values, measurement on castings.
2) For the wall thickness g [mm]; $30 < g \leq 60$.
3) For the wall thickness g [mm]; $60 < g \leq 200$.

The 0.94% molybdenum content favors the formation of a larger amount of pearlite in the matrix. In the first case, the amount of silicon is 3.6% and in the second, 4.1%. The amount of manganese is 0.15% in the first one, and 0.38 in the second [9, 10].

The high molybdenum content increases the chances of unfavorable M_6C and M_7C_3 carbides at the grain boundaries. The heat treatment applied to SiMo iron castings is able to eliminate secondary carbides and pearlite, leading to the ferritization of the matrix. As can be seen from the phase diagram, M_7C_3 carbides are only stable down to a temperature of less than about 300°C. After heat treatment, ferrite saturated with molybdenum emits fine dispersion carbides in its grains and not at the grain boundaries, which has a positive effect on the mechanical properties. This heat treatment does not work with M_6C primary carbides which are stable and only dissolve above about 1100°C [9].

1.2. Mechanical properties and influence of Mo, Si, Al, and Cr

SiMo ductile iron castings must exhibit increased mechanical properties at high temperatures and the addition of molybdenum increases the temperature range of such castings. Molybdenum also increases the tensile strength UTS of SiMo cast iron. It is an element that increase the amount of pearlite in the matrix, which, at higher contents (about 1% mas.), may have an unfavorable effect on the structure. As mentioned earlier, precipitation of pearlite at the grain boundaries decreases the tensile strength and ductility and a heat treatment to obtain ferrite in the matrix may be necessary. The high content of silicon in this type of cast iron partially neutralizes the harmful effect of molybdenum on the structure and properties, increasing the ability to ferrite cast iron. As a result, the elongation increases. Due to its properties, silicon causes that the amount of carbon in cast iron in foundry practice does not exceed 3% mass, especially with contents above 4.5% Si mas. [11–14].

The research [12] showed that cast iron with the addition of 4.0% Si and 1.4% Mo has good mechanical properties at a temperature of up to 600°C.

Chromium as an additive to cast iron increases resistance to high temperature [15]. As a component of nickel-chromium cast iron in the amount of up to 2%, it also has a positive effect on hardness [16]. Chromium amplifies the tendency of cast iron to metastable crystallization with precipitates of carbides, which may necessitate the production of cast iron with the addition of aluminum.

Aluminum improves the graphitization of cast iron. With an aluminum content of 3.2–3.8%, the matrix is ferritic. Such an increase in the ferritization capacity of cast iron can help to obtain the appropriate structure of SiMo cast iron while increasing its resistance to high temperatures [15, 17–19].

2. RESEARCH METHODOLOGY

The initial cast iron was melted twice in a medium-frequency induction furnace with a chamotte-graphite crucible with a capacity of 15 kg, which is provided by the Experimental Foundry of the Faculty of Foundry Engineering, AGH University of Science and Technology. At the end of each melt, the liquid cast iron was superheated to a temperature of 1490–1500 °C and this was maintained for a period of 3 minutes. The procedure of inoculation liquid metal was performed by introducing a zirconium inoculant with a granulation from 2 to 5 mm, by Elkem. The material had been selected to prepare ductile iron castings with an increased content of silicon and molybdenum. Nodularization treatment was prepared by means of the bell method using a blend containing 17% magnesium. A stepped sample (Fig. 1. and Fig. 2.), and a sample for chemical composition has been cast of each melt. The chemical composition was checked ona Bruker spectrometer. Metallographic, and tensile strength samples were cut from the prepared castings (Fig. 3.).

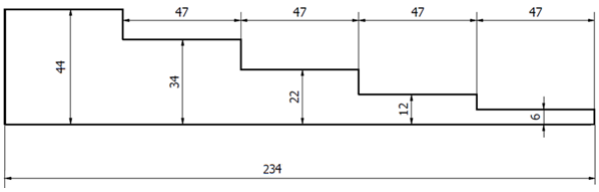

Fig. 1. Research sample dimensions

Fig. 2. Research samples of cast iron

Fig. 3. Gray iron tensile strength sample made according to the customer's standard. Diameter of the sample D = 6 mm, length without fixings L = 15 mm

3. RESULTS

The chemical composition of the cast samples is shown in Table 2. Sample 1 and 2 were made of the same heat, while sample 3 was at another heat. In both cases, the bell spheroidization was attempted, but due to the high concentration of magnesium in the spheroidizer (17%), the attempt was unsuccessful. Further research mainly concerns mainly the matrix and carbide precipitates.

Table 2
Chemical compositions of obtained cast irons

Sample number	Content [%]								
	C	Si	Mo	Mn	Cr	S	Al	Cu	Mg
1 2	2.44	5.67	0.77	0.42	0.08	0.01	0.01	0.12	<0.015
3	2.62	5.54	0.79	0.39	0.09	0.018	0.01	0.09	<0.015

The results of the tensile strength UTS tests are presented in Table 3. The lack of the elongation parameter is caused by the overly small size of the sample and the inability to install an extensometer.

Table 3
Tensile strength of obtained cast irons

Sample number	Step number	Wall thickness [mm]	R_m [MPa]
1	2	12	325
	3	22	297
2	2	12	306
	3	22	261
3	2	12	203
	3	22	162

The microstructure of each sample is shown in Figure 4. All photos are taken at 100× magnification. The pictures of non-etched structures clearly show that it is gray cast iron. We are dealing here with the predominant amount of type A flake graphite. In the wall thickness of 34 mm, it is especially noticeable that there are also type C graphite precipitates in the microstructure.

After etching the structures with nitrile, it can be seen that the cast iron matrix is practically pure ferrite. Pearlite appears at the grain boundaries, but there is not much of it. The greatest amount of pearlite at the grain boundaries is found in sample 3. Moreover, the precipitates of flake graphite in this sample are the largest and their amount is the highest.

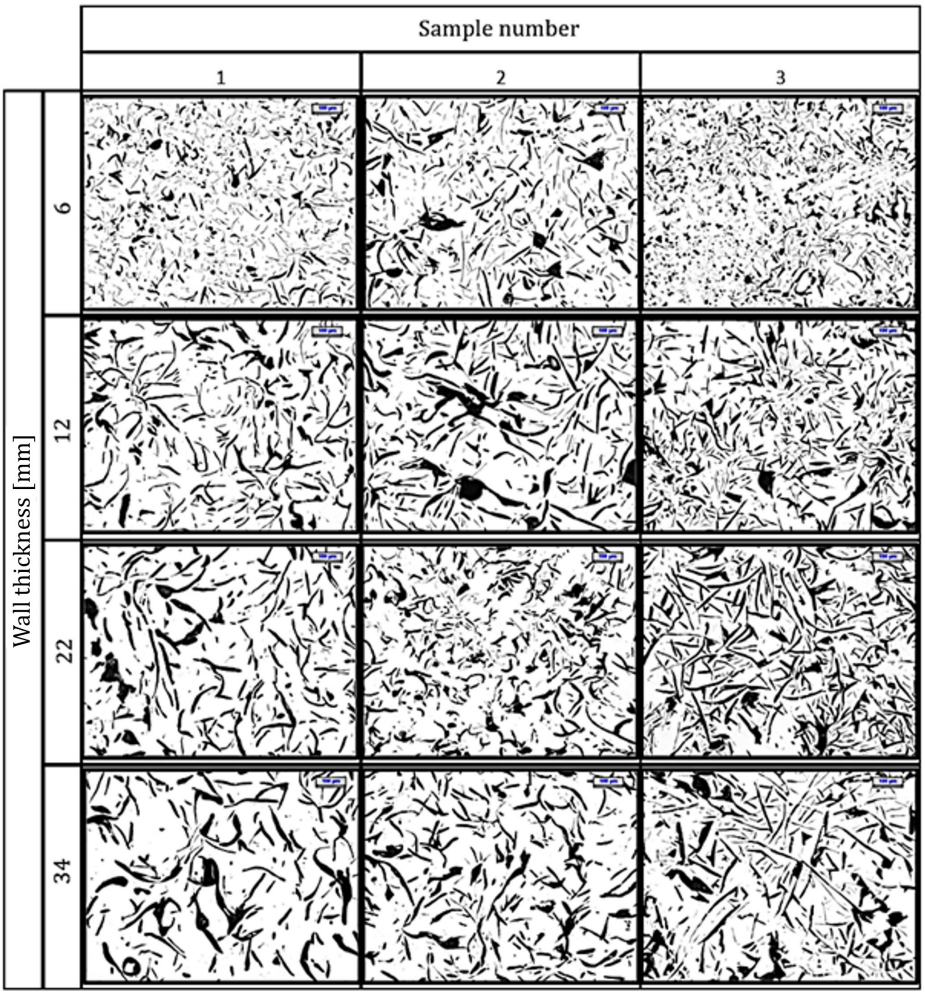

Fig. 4. Microstructures of prepared samples, non-etched, magnification 100×

This mainly applies to thicker walls, since sample 3 has very fine graphites on the 6 mm wall. Only M_6C primary carbides can be seen at the grain boundaries. The etched structure is shown in Figure 5.

Sample 2 has an evenly distributed graphite and their size is more uniform than in samples 1 and 3. The graphite precipitates themselves are less than in sample 3, instead carbide clusters were found. In this sample, precipitation of M_6C carbides and small amounts of M_7C_3 carbides can be seen as shown in Figure 6.

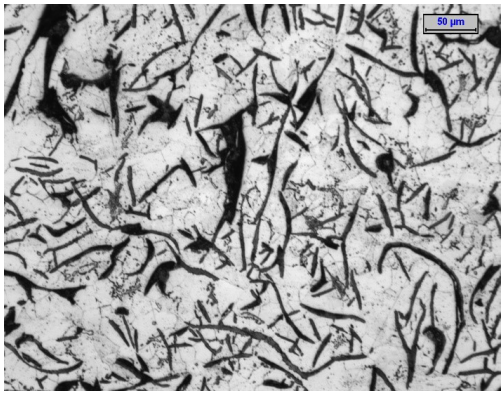

Fig. 5. Microstructures sample 3 in 22 mm wall thickness. Etched, magnification 200×

a)

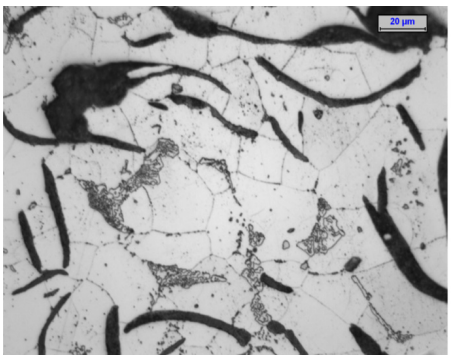

b)

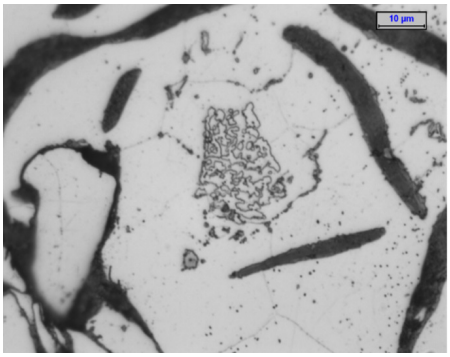

Fig. 6. Precipitations of M6C carbides at the grain boundaries of sample 2 in 22 mm wall thickness. Etched, magnification 500× (a) and 1000× (b)

Sample 1 has the least amount of pearlite at the grain boundaries, while there are large clusters of carbide precipitates. Here, the largest amount of M_7C_3 carbides occurs, but the vast majority of carbide precipitates are M_6C. An exemplary structure at a magnification of 500× is shown in Figure 7.

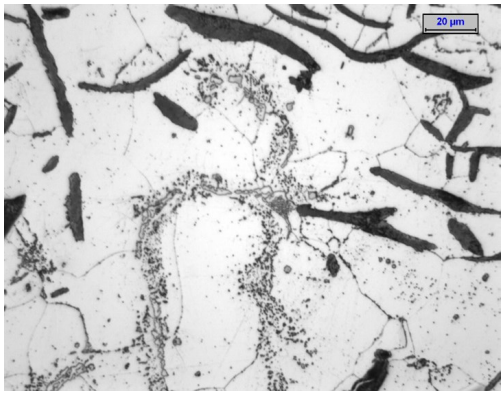

Fig. 7. Precipitations of M_6C and M_7C_3 carbides at the grain boundaries of sample 1, 34 mm wall thickness. Etched, magnification 500×

4. CONCLUSIONS

By analyzing the research results, the following conclusions can be drawn:

- Spheroidization with a 17% Mg blend is a bad solution in such a small crucible. Subsequent treatments will be performed with an alloy containing no more than 6% Mg.
- It is possible to obtain a gray cast iron structure with an increased content of silicon and molybdenum with the presence of M_6C and M_7C_3 carbides.
- Samples with finer particles of graphite in their structure (samples 1 and 2) are characterized by higher strength properties (UTS).
- Due to the absence of nodular graphite in the structure, cast iron has a much lower tensile strength than expected.
- The higher carbon content with the simultaneous high silicon content in sample 3 resulted in the formation of a large amount of flake graphite particles, which weakened the structure, leading to lower mechanical properties.
- The obtained cast iron could be an interesting alternative to cast iron used for castings of brake discs and pads, if good anti-abrasive and anti-corrosion properties are confirmed.
- In subsequent tests, heat treatment of the obtained samples should be carried out in order to try to eliminate large precipitates of carbides at the grain boundaries.

REFERENCES

[1] Lekakh S.N., Buchely M., O'Malley R., Godlewski L. & Mei Li. (2021). Thermo-cycling fatigue of SiMo ductile iron using a modified thermo-mechanical test. *International Journal of Fatigue*, 148, 106218. Doi: https://doi.org/10.1016/j.ijfatigue.2021.106218.

[2] Castro Güiza G.M., Hormaza W., Galvis E.A.R. & Mïndez Moreno L.M. (2017). Bending overload and thermal fatigue fractures in a cast exhaust manifold. *Engineering Failure Analysis*, 82, 138–148. Doi: https://doi.org/10.1016/j.engfailanal.2017.08.016.

[3] Karnik A.Y. & Shelby M.H. (2010). Effect of Exhaust Gas Temperature Limits on the Peak Power Performance of a Turbocharged Gasoline Engine. *Journal of Engineering for Gas Turbines and Power*, 132(11), 112801. Doi: https://doi.org/10.1115/1.4000856.

[4] Rathnaraj D.J. (2012). Thermomechanical fatigue analysis of stainless steel exhaust manifolds. *International Journal of Engineering, Science and Technology*, 2(2), 265.

[5] Black B., Burger G., Logan R., Perrin R. & Gundlach R. (2002). Microstructure and Dimensional Stability in Si-Mo Ductile Irons for Elevated Temperature Applications. *SAE Technical Paper*. 2002-01-2115. Doi: https://doi.org/10.4271/2002-01-2115.

[6] Dorula J., Kopyciński D., Guzik E., Szczęsny A. & Gurgul D. (2021). The Influence of Undercooling ΔT on the Structure and Tensile Strength of Gray Cast Iron. *Materials*, 14(21), 6682. Doi: https://doi.org/10.3390/ma14216682.

[7] Dawi K., Favergeon J. & Moulin G. (2008). High Temperature Corrosion of the Si-Mo Cast Iron in Exhaust Atmosphere. *Materials Science Forum*, 595–598, 743–751. Doi: https://doi.org/10.4028/www.scientific.net/msf.595-598.743.

[8] Standard EN 16124:2012. Founding – Low-alloyed ferritic spheroidal graphite cast irons for elevated temperature applications.

[9] Çelik G.A., Tzini M.-I.T., Polat Ş. Aristeidakis J.S., Atapek Ş.H., Sarafoglou P.I. & Haidemenopoulos G.N. (2021). Simulation and analysis of the solidification characteristics of a Si-Mo ductile iron. *Journal of Mining and Metallurgy Section B: Metallurgy*, 57(1), 53–62. Doi: https://doi.org/10.2298/JMMB200717003C.

[10] Vaško A. (2020). Comparison of mechanical and fatigue properties of SiMo- and SiCu-types of nodular cast iron. *Materialstoday: Proceedings*, 32(2), 168–173. Doi: https://doi.org/10.1016/j.matpr.2020.04.184.

[11] Åberg L.M. & Hartung C. (2012). Solidification of SiMo Nodular Cast Iron for High Temperature Applications. Indian Institute of Metals. *Transactions of the Indian Institute of Metals*, 65(6), 633–636. Doi: https://doi.org/10.1007/s12666-012-0216-8.

[12] Matteis P., Scavino G., Castello A. & Firrao D. (2014). High temperature fatigue properties of Si-Mo Ductile Cast iron. *Procedia Materials Science*, 3, 2154–2159. Doi: https://doi.org/10.1016/j.mspro.2014.06.349.

[13] Górny M., Kawalec M., Gracz B. & Tupaj M. (2021). Influence of Cooling Rate on Microstructure Formation of Si-Mo Ductile Iron Castings. *Metals*, 11(10), 1634. Doi: https://doi.org/10.3390/met11101634.

[14] Angella G., Taloni M., Donnini R. & Zanardi F. (2022). The Correlation between Solidification Rates, Microstructure Integrity and Tensile Plastic Behaviour in 4.2 wt.% Silicon Strengthened Ductile Iron. *Journal of Casting & Materials Engineering*, 6(1), 1–8. Doi: https://doi.org/10.7494/jcme.2022.6.1.1.

[15] Dyrlaga Ł., Kopyciński D., Guzik E. & Szczęsny A. (2021). Struktura i właściwości żeliwa odpornego na działanie wysokiej temperatury oraz na zużycie ścierne. In: J.J. Sobczak (red.), *Metalurgia 2020*, 326–343.

[16] Mourad M., El-Hadad S. & Ibrahim M.M. (2015). Effects of Molybdenum Addition on the Microstructure and Mechanical Properties of Ni-Hard White Cast Iron. *Transactions of the Indian Institute of Metals*, 68, 715–722. Doi: https://doi.org/10.1007/s12666-014-0504-6.

[17] Kashani S.M. & Boutorabi S.M.A. (2009). As-Cast Acicular Ductile Aluminum Cast Iron. *Journal of Iron and Steel Research International*, 16(6), 23–28. Doi: https://doi.org/10.1016/S1006-706X(10)60022-2.

[18] Gilewski R., Kopyciński D., Guzik E. & Szczęsny A. (2021). An Evaluation of the Microstructure of High-Aluminum Cast Iron in Terms of the Replacement of Aluminum Carbide with Titanium Carbide or Tungsten Carbide. *Applied Sciences,* 11(20), 9527. Doi: https://doi.org/10.3390/app11209527.

[19] Gilewski R., Kopyciński D., Guzik E. & Szczęsny A. (2021). Shaping the Microstructure of High-Aluminum Cast Iron in Terms of the Phenomenon of Spontaneous Decomposition Generated by the Presence of Aluminum Carbide. *Materials*, 14(20), 5993. Doi: https://doi.org/10.3390/ma14205993.